Korean J. Chem. Eng., 40(7), 1672-1685 (2023)
DOI: 10.1007/s11814-022-1369-8

pISSN: 0256-1115
eISSN: 1975-7220

Applicability of HFSLM for Nd(III) recovery via organophosphorus carrier: A conceptual DFT approach towards structural chemistry, mechanistic investigation and transport behavior

Vanee Mohdee*, Nisit Sulaiman*, Wikorn Punyain,†, and Ura Pancharoen*,†**

*Department of Chemical Engineering, Faculty of Engineering, Chulalongkorn University, Bangkok 10330, Thailand
**Department of Chemistry and NU-Research Center for Petroleum, Petrochemicals and Advanced Materials, Faculty of Science, Naresuan University, Phitsanulok, 65000, Thailand
(*Received 26 September 2022 • Revised 18 November 2022 • Accepted 8 December 2022*)

Abstract−This work highlights the enrichment of Nd(III) via hollow fiber supported liquid membrane (HFSLM). In terms of the practicability to separate Nd(III), the influence of significant factors and the behavior of different carrier concentrations were evaluated. Using Di-(2-ethylhexyl)phosphoric acid (D2EHPA) as a ligand carrier, high enrichment performance of Nd(III) can be achieved. Under optimum conditions, extraction and stripping of Nd(III) reached 99.80% and 78.58%, respectively. Further, the active Nd(III) transportation was analyzed to emphasize key parameters that govern the separation process. The values k_{ex} (cm/s) and Δ_{ex} (%) were found to be 1.38×10^{-5} and 81.20, respectively, indicating the mass transfer due to chemical reaction is the controlling step. Density-functional theory (DFT) was applied to explore the interaction mechanisms from a microscopic viewpoint. Comprehensive analysis was made to achieve better insight regarding the reaction mechanisms and the structural chemistry underlying the process of Nd(III) enrichment.

Keywords: HFSLM, Neodymium Separation, DFT, D2EHPA, Mass Transfer

INTRODUCTION

Neodymium (Nd) is one of the reactive lanthanides that is categorized in the rare earth elements group (REEs). It has been extensively used in a wide range of applications, including the manufacturing of several high-tech devices [1,2]. Especially, Nd is a vital chemical element in permanent magnet appliances owing to its particular spectroscopic and magnetic properties [3-6]. Due to their high demand along with their limited resources, REEs are listed as critical raw materials of strategic importance [5,7]. In consequence, the separation and recovery of Nd is indispensable.

Different hydrometallurgical processes have been applied for the separation of Nd(III) [6,8,9]. However, these conventional hydrometallurgical methods have been found to have some inherent limitations and practical difficulties as well as requiring several steps [2,10,11]. Yoon et al. [11] reported that nine stages of solvent extraction are needed to complete the separation of Nd(III). Owing to high chemical utilization of such methods, high quantities of chemical waste have been generated. Thereby, the disposal of spent chemical reagents is problematic [9,12]. The drawbacks of conventional methods are summarized in the Supplementary Material (Table S1) [1].

Recently, hollow fiber membrane technology has attracted considerable attention, as such a system enables both extraction and stripping reactions to occur simultaneously [13]. This process can selectively separate target specie at a trace concentration level and still provide high efficiency. When hollow fiber supported liquid membrane (HFSLM) is utilized, a small footprint is generated because of high interfacial areas per unit volume [14,15]. HFSLM can be regarded as a promising system for "as low as reasonably achievable" mass separation processes [16]. Of these technological challenging methods, the membrane extraction system is especially significant, having several advantages over conventional methods. HFSLM is known to have lower operating costs, less energy consumption and less chemical reagents. On account of the reusability of the liquid membrane, HFSLM can be regarded as a green technology over conventional methods following an environmentally benign strategy [10,17-19]. Further, this technology exhibits a remarkable potential for large scale applications [18,20]. Hence, the major challenge in order to assess this technology is to tackle the membrane fouling issue [21,22]. Many researchers have attempted to tackle this problem as well as improve the separation performance; thereby membrane properties, hydrodynamic conditions and operating conditions need to be carried out [21,22]. Some points of perspective must be considered in order to adopt industrial scale hollow fiber membrane technology such as the membrane availability, membrane fouling, technical issues and the cost aspect [22]. In consideration of this, sustainable strategies for the separation of Nd are imperative for both fundamental and practical viewpoints. In Table 1, a summary of previous works on Nd(III) separation is presented.

As a promising sub-area of chemistry, computational chemistry provides a better understanding of the behavior of atoms and molecules. By applying computational chemistry, useful data--molecular geometries, reactivity, spectra, structural chemistry and other prop-

†To whom correspondence should be addressed.
E-mail: kraiwanp@nu.ac.th, ura.p@chula.ac.th

Table 1. Summary of previous works on Nd(III) separation

Feed solution	Separation methods	Materials/Reagents	Separation efficiency
Synthetic solution [5]	Solvent extraction	Cyanex272	Small amounts of Nd(III) were extracted in three stages at A/O ratio=1/1
Synthetic solution [6]	Solvent extraction and recovery with direct electrodeposition	Synthetic of octylphosphite-based ILs/electrodeposition at −2 V, 313 K	%Extraction=98 %Recovery=48
Synthetic solution [7]	Adsorption	Superparamagnetic nanoparticles	>99%
Synthetic solution [8]	Solvent extraction	Tetrabutylphosphonate nitrate	%Extraction=99.7
Synthetic solution [9]	Adsorption	Bis(2-ethylhexyl) phosphate-particle-packed cartridge	%Purity=95
Waste permanent magnets leach liquor [12]	HFSLM	D2EHPA	%Extraction=58.62 %Recovery=63.13
Synthetic solution [23]	HFSLM	D2EHPA mixed TOPO	%Extraction=94.5 %Recovery=85.1

erties--are assessed. However, since an appropriate picture at the molecular level is still lacking, an analysis regarding reaction mechanisms that occur in separation processes has been investigated [24-27]. Computational chemistry based on quantum mechanical simulation is increasingly probed to tackle unanswered questions in the process of metals separation.

The purpose of this work is to evaluate the versatility of HFSLM as a technologically challenging system for the enrichment of Nd(III) from aqueous solutions. Significant variables in the process have been duly investigated, such as concentration of D2EHPA as extractant, pH of aqueous feed solutions, initial concentration of Nd(III) and concentration of HNO_3 as stripping solution. Equilibrium slope analysis has been employed to determine the stoichiometry of metal/extractant and metal/strippant associated in the reactions. Transport of active Nd(III) ions through HFSLM has also been examined together with the analysis of diffusional parameters to find the influential parameters governing the separation process.

To the best of our knowledge, our current findings expand upon previous work through in-depth investigation into the interaction behavior between Nd(III) and D2EHPA in order to analyze the mechanisms underlying the enrichment of Nd(III). Herein, the molecular structure and interaction mechanisms are studied from a microscopic viewpoint, which provides the basis for screening efficient extractants. An attempt has been made to gain a better understanding of reaction mechanisms and the structural chemistry of the complexes formed via DFT. It is seen that computational chemistry can overcome the limitation of previous approaches.

EXPERIMENTAL

1. Reagents and Chemical Compounds

Commercial neodymium(III) oxide (Nd_2O_3) (Sigma-Aldrich, Poland) was used to synthesize the aqueous feed solutions. Di-(2-ethylhexyl)phosphoric acid (D2EHPA, $C_{16}H_{35}O_4P$) obtained from Sigma-Aldrich (Poland) was used as an extractant to examine the extractability of Nd(III). Kerosene (Thai Oil Public Company Limited, Thailand) was used as diluent. Nitric acid (HNO_3) supplied by Merck (Singapore) was used as stripping solution. Aqueous solutions in the experiment were prepared using deionized water (Millipore, USA). All reagents used in this experiment were of analytical grade and used without further purification.

2. Apparatus

HFSLM applied in this work was a 2.5×8 inch Liqui-Cel® Extra-Flow membrane contactor manufactured by Hoechst Celanese, USA. The module composed of Celgard®x-40 microporous polypropylenes fibers woven into the fabric was used. In Table 2, characteristics of the HF module are provided.

3. Experimental Procedures

The laboratory scale consists of the HF module connected to the reservoirs. Peristaltic pumps were used continuously to recir-

Table 2. Characteristics of the hollow fiber module

Properties	Descriptions
Inside diameter of hollow fiber	240 μm
Outside diameter of hollow fiber	300 μm
Effective length of hollow fiber (L)	15 cm
Number of hollow fibers (N)	35,000
Average pore size	0.03 μm
Size of pore	0.05 μm
Porosity (ε)	30%
Effective surface area (A)	1.4 m^2
Area per unit volume	29.3 cm^2 cm^{-3}
Module diameter	6.3 cm
Module length	20.3 cm
Tortuosity factor	2.6
Maximum pressure difference	4.2 kg cm^{-2} (60 psi)
Operating temperature	273-333 K

Note: The characteristics of the HF module are as stated by supplier (Hoechst Celanese, USA).

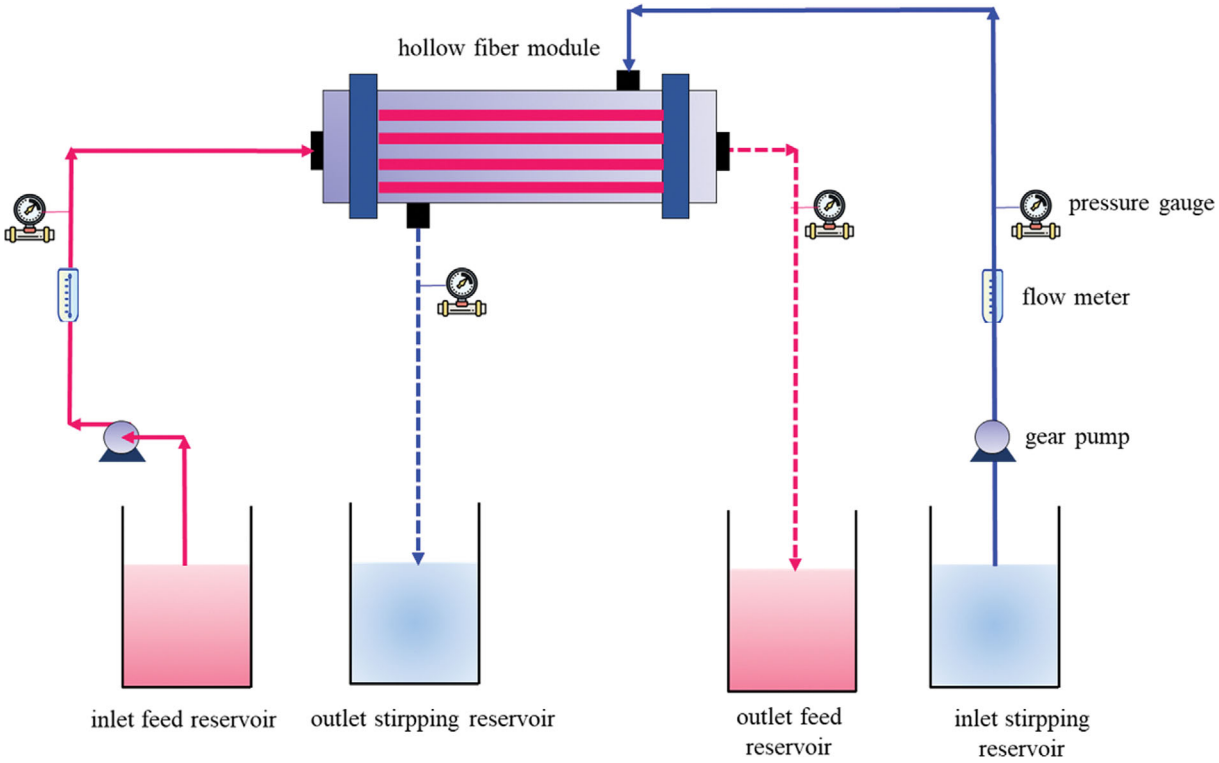

Fig. 1. Schematic diagram of laboratory scale HFSLM setup; counter-current flow for once-through operation mode.

culate the solutions fed through the HF module. For the LMs phase, D2EHPA dissolved in kerosene was employed. The LMs were simultaneously pumped into the tube and shell sides of the HF module for 40 min to ensure that the LMs were entirely immobilized in the micropores of the hollow fibers. Subsequently, distilled water was fed through the system to wash out the excess LMs. After that, both aqueous solutions (feed and stripping) were driven counter-currently into the tube and shell sides of the HF module, respectively. The sampling aqueous solutions were collected and analyzed for Nd(III) content using UV-Vis Spectroscopy (6450 UV/VIS Spectrophotometer, Jenway, Labquip International Limited). The UV-Vis spectroscopic determination of Nd(III) was at 655 nm, using Arsenazo III reagent. The experiments were carried out for 1 h and conducted in an open system under atmospheric pressure (101.325 kPa) for practicality and ease of use. In Fig. 1, the laboratory scale of the HFSLM setup is depicted.

4. Measurement of Enrichment Efficiency

The enrichment efficiency of Nd(III) can be determined in terms of percentages of extraction and stripping, as expressed in Eqs. (1)-(2):

$$\%\text{Extraction} = \frac{C_{f,\,in} - C_{f,\,out}}{C_{f,\,in}} \times 100 \tag{1}$$

$$\%\text{Stripping} = \frac{C_{s,\,out}}{C_{f,\,in}} \times 100 \tag{2}$$

where $C_{f,in}$ is the initial concentration of neodymium ions in the feed solution, $C_{f,out}$ and $C_{s,out}$ are the outlet concentration of neodymium ions in the feed and stripping sides, respectively.

5. Theoretical Background

5-1. Carrier Facilitated Transport

It is acknowledged that mass transport in liquid membranes (LMs) is considered as carrier-mediated transport [18]. Fundamentally, HFSLM consists of three stages: aqueous feed phase, LMs phase and stripping phase. Both aqueous solutions, i.e., feed (containing target metal specie) and stripping are in contact with the LMs, which act as a barrier to separate these two solutions [15]. Hence, the transport phenomena of the active Nd(III) that occur in the HFSLM system can be described as follows:

Step I Target Nd(III) ions containing in aqueous feed solutions diffuse from the bulk feed phase through the stagnant layer of the feed side to the interface between the feed phase and the LMs phase. Thereby, extraction reaction occurs and an organometallic complex of Nd(III) in the loaded organophosphorus ligand is formed. The extraction mechanisms of Nd(III) via D2EHPA extractant can be expressed as follows [28,29]:

$$Nd^{3+}_{aq} + 3(HR)_{2,\,org} \underset{k'_{ex}}{\overset{k_{ex}}{\leftrightarrow}} NdR_3 \cdot (HR)_{3,\,org} + 3H^{+}_{aq} \tag{3}$$

The equilibrium constant of Nd(III) extraction as well as the reaction rate of Nd(III) in the loaded D2EHPA carrier formation can be simplified, as shown in Eqs. (4)-(6), respectively:

$$K_{ex} = \frac{[NdR_3 \cdot (HR)_3][H^+]^3}{[Nd^{3+}][(HR)_2]^3} \tag{4}$$

$$r_{forward} = k_{ex}\left(\frac{[Nd^{3+}][HR_2]^3}{[H^+]^3} - \frac{[NdR_3 \cdot (HR)_3]}{K_{ex}}\right) \tag{5}$$

$$r_{backward} = k'_{ex}\left([NdR_3\cdot(HR)_3] - K_{ex}\frac{[Nd^{3+}][HR_2]^3}{[H^+]^3}\right) \quad (6)$$

Step II The organometallic complex of Nd(III) in the loaded organophosphorus ligand is transported across the LMs, due to the concentration gradient, to the interface between the LMs phase and stripping phase.

Step III Stripping reaction simultaneously occurs at the interface between the LMs phase and stripping phase. Target metal ions (Nd(III)) diffuse and pass by the stripping layer; the ligand carrier (D2EHPA) is regenerated by diffusing back to the Feed/LMs interface where it is ready to react with other metal ions. Subsequently, Nd(III) is released into the stripping solutions. The stripping mechanism of Nd(III) is shown below [19,28]:

$$NdR_3\cdot(HR)_{3,\,org} + 3H^+_{aq} \underset{k'_{st}}{\overset{k_{st}}{\leftrightarrow}} Nd^{3+}_{aq} + 3(HR)_{2,\,org} \quad (7)$$

Accordingly, the equilibrium constant of Nd(III) stripping reaction becomes:

$$K_{st} = \frac{[Nd^{3+}][(HR)_2]^3}{[NdR_3\cdot(HR)_3][H^+]^3} \quad (8)$$

5-2. Diffusion Flux Model: Numerical Approach

- Aqueous feed phase

The diffusion of Nd(III) from the bulk feed phase to the stagnant layer of the feed side can be expressed by Fick's law as follows:

$$J_{aq} = \Delta_{aq}^{-1}([Nd^{3+}]_f - [Nd^{3+}]_{f/i}) \quad (9)$$

where Δ_{aq}^{-1} is the aqueous phase resistance, and $[Nd^{3+}]_f$ and $[Nd^{3+}]_{f/i}$ are the concentrations of Nd(III) in the bulk feed solution and at the feed/LMs interface, respectively.

- LMs phase

The diffusion of Nd(III) in the loaded D2EHPA carrier complex through the LMs phase can be written as follows:

$$J_{LMs} = \Delta_{LMs}^{-1}([Nd^{3+}]_{f/LMs} - [Nd^{3+}]_{LMs/s}) \quad (10)$$

where Δ_{LMs}^{-1} is the organic phase resistance, which results from the diffusion through the LMs phase. $[Nd^{3+}]_{f/LMs}$ and $[Nd^{3+}]_{LMs/s}$ are the concentrations of Nd(III) in the loaded D2EHPA carrier complex at the feed/LMs and LMs/stripping interfaces, respectively.

It has been reported that the distribution of Nd(III) between the LMs phase and stripping phase is much lower than that between the feed phase and LMs phase [30]. As a consequence, the concentration of $[Nd^{3+}]_{LMs/s}$ can be neglected. Thus, Eq. (10) can be simplified as:

$$J_{LMs} = \Delta_{LMs}^{-1}\cdot[Nd^{3+}]_{f/LMs} \quad (11)$$

The extraction reaction, as expressed in Eq. (3), is considered to be fast compared to the diffusion rate. Hence, the equilibrium concentration at the interface can be related, as outlined in Eq. (4) [30]. At steady state, where $J_{aq}=J_{LMs}=J$, the expression of flux can be obtained as shown in Eq. (12):

$$J = \frac{K_{ex}[(HR)_2]^3}{\Delta_{LMs}[H^+]^3 + \Delta_{aq}K_{ex}[(HR)_2]^3}\cdot[Nd^{3+}]_f \quad (12)$$

In terms of the permeability coefficient (P), the equation can be defined as [30,31]:

$$P = \frac{J}{[Nd^{3+}]_f} = \frac{K_{ex}[(HR)_2]^3}{\Delta_{LMs}[H^+]^3 + \Delta_{aq}K_{ex}[(HR)_2]^3} \quad (13)$$

or

$$\frac{1}{P} = \Delta_{aq} + \frac{\Delta_{LMs}}{K_{ex}[(HR)_2]^3([H^+]^3)^{-1}}$$

$$= \Delta_{aq} + \frac{\Delta_{LMs}}{\{[NdR_3\cdot(HR)_3]/[Nd^{3+}]\}} \quad (14)$$

or $$\frac{1}{P} = \Delta_{aq} + \frac{\Delta_{LMs}}{D} \quad (15)$$

where D is the distribution of Nd(III) at various carrier concentrations. The values of mass transfer coefficients in both aqueous and LMs phases can be obtained via the fitted slope by plotting 1/P versus 1/m; a straight line is expected with slope Δ_{LMs} and intercept Δ_{aq}.

The molar flux of Nd(III) across HFSLM can be calculated, as shown below: [32]

$$J = -\frac{V}{A}\frac{dC}{dt} \quad (16)$$

where A is the membrane area and V is the volume of aqueous feed solution.

Thus,

$$\frac{d([Nd]^{3+})}{[Nd^{3+}]} = -\frac{PA}{V}dt \quad (17)$$

As a consequence, the transportation of Nd(III) across HFSLM in terms of flux and permeability coefficient can be determined via Eqs. (18)-(19):

$$J = \frac{V\{[Nd^{3+}]_{initial} - [Nd^{3+}]_t\}}{At} \quad (18)$$

$$P = \frac{V\{\ln[Nd^{3+}]_{initial}/[Nd^{3+}]_t\}}{At} \quad (19)$$

where, t is the elapsed time, $[Nd^{3+}]_{initial}$ and $[Nd^{3+}]_t$ are the concentrations of Nd(III) at initial time and at time t, respectively.

In Fig. 2, a schematic diagram of couple facilitated counter-transport of Nd(III) across HFSLM system is presented.

5-3. Mass Transport of Nd(III) in a Hollow Fiber (HF) Module

During the process of active Nd(III) transport through the HFSLM system, six individual mass transfer coefficients are taken into consideration [33]:

(i) The mass transfer coefficient in the aqueous feed phase (k_{af}): it is the mass transfer when the aqueous feed solution is flowing through the HF lumen.

(ii) The mass transfer coefficient due to the extraction reaction (k_{ex}).

(iii) The mass transfer coefficient of the organometallic complex in the LMs (k_{LMs}): it is due to the diffusion of the organometallic complex through the LMs, which is immobilized in the pores of the HF.

(iv) The mass transfer coefficient in the shell side (k_o): it is due to the flow of the stripping solution in the shell side of the HF

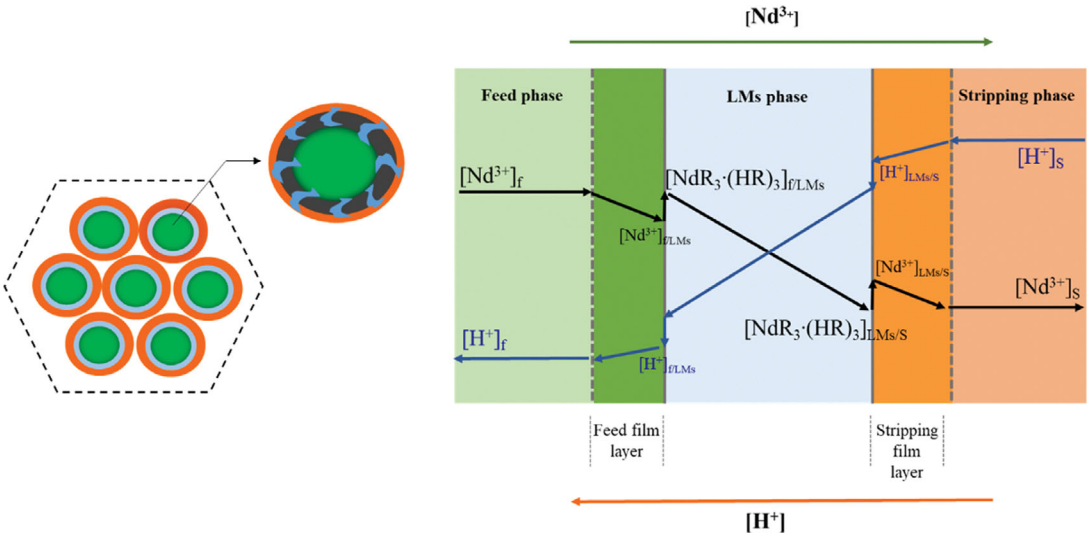

Fig. 2. Schematic diagram of Nd(III) transportation across HFSLM system.

module.

(v) The mass transfer coefficient due to the stripping reaction (k_{st}).

(vi) The mass transfer coefficient due to the receiver phase/strip side (k_{as}).

The reciprocal of the overall mass transfer coefficient (K) can be written as shown in Eq. (20):

$$\frac{1}{K}=\frac{1}{k_{af}}+\frac{1}{k_{ex}}+\frac{1}{m_f k_{LMs}}+\frac{1}{m_s k_o}+\frac{1}{m_s k_{st}}+\frac{1}{(m_s/k_{st})k_{as}} \quad (20)$$

Thus, the contribution of mass transfer coefficient due to the stripping reaction is usually neglected due to the instantaneous reaction during the process of separation via HFSLM [33]. Therefore, the equation representing the overall mass transfer coefficient of the transported species across HFSLM system can be expressed as follows:

$$\frac{1}{K}=\frac{1}{k_{af}}+\frac{1}{k_{ex}}+\frac{1}{m_f k_{LMs}}+\frac{1}{m_s k_o} \quad (21)$$

where m is the partition coefficient. The partition coefficient of Nd(III) between the LMs and the aqueous feed phase (m_f) can be calculated, as follows:

$$m_f=\frac{[NdR_3\cdot(HR)_3]}{[Nd^{3+}]_f} \quad (22)$$

Hence, the mass transfer coefficients in each phase can be determined using the following equations [19,33,34]:

$$k_{af}=1.62\frac{\mathcal{D}_{Nd,\,aq.}}{2r_i}\left(\frac{4r_i^2 v_f}{L\mathcal{D}_{Nd,\,aq.}}\right)^{0.33} \quad (23)$$

$$k_{ex,\,equilibrium}=\frac{1}{k_{ex}[Nd^{3+}][(HR)_2]^2-k_{st}[NdR_3\cdot(HR)_3][H^+]^3} \quad (24)$$

$$k_{LMs}=\frac{\varepsilon\mathcal{D}_{LMs}}{\pi r_i \ln(r_o/r_i)} \quad (25)$$

$$k_o=1.25\frac{\mathcal{D}_{Nd,\,aq.}}{d_h^{0.07}}\left(\frac{d_h v_s}{\upsilon L}\right)^{0.93}\left(\frac{\upsilon}{\mathcal{D}_{Nd,\,aq.}}\right)^{0.33} \quad (26)$$

where v_f and v_s are the linear velocities of both the aqueous feed and stripping solutions (cm/s), respectively. r_i and r_o are the inner and outer radius of HF (cm), respectively. $\mathcal{D}_{Nd,\,aq.}$ is the diffusion coefficient of Nd(III) in the aqueous solution (5.48×10^{-5} cm^2/s). $\mathcal{D}_{LMs}$ is the diffusivity of Nd(III) in LMs (cm^2/s). υ is the kinetic viscosity of LMs (cm^2/s).

RESULTS AND DISCUSSION

1. Analysis on Selected Extractant and Solvent

The significant physicochemical properties of extractant to be applied in the separation process are (i) low solubility in the aqueous phase and at the same time very high solubility in organic diluents, (ii) density as well as viscosity should be low, and (*iii*) high stability [11].

D2EHPA is one of the leading effective extractants, which has been widely applied in hydrometallurgical processing involving diverse types of metal separation [3,12,23,28]. As an acidic extractant, D2EHPA exhibits high extraction power [12]. The functional groups: P=O and P···O contained in the D2EHPA structure are able to ascertain the superior performance in terms of the formation of complexes with rare earth elements [35]. The functional group of 2-ethylhexyl contained in D2EHPA favor the solubility in organic diluents and the low solubility of D2EHPA in water, suggesting D2EHPA is a suitable extractant in the process of separation and purification [36]. Srirachat et al. [37] reported that D2EHPA extractant dissolved in kerosene diluent exhibited the strongest interaction among other solvents (i.e., n-heptane, chlorobenzene and 1-octanol) owing to its large hydrophobic molar volume. The intermolecular force between D2EHPA and kerosene is found to be London force. Such attraction force occurs due to the interaction between two non-polar groups of 2-ethylhexyl in D2EHPA and hydrocarbon chain in kerosene. Further, the majority of using D2EHPA in the process of REEs separation is mainly due to its distinguishing properties: high sorption rate, chemical stability, and low aqueous solubility [38].

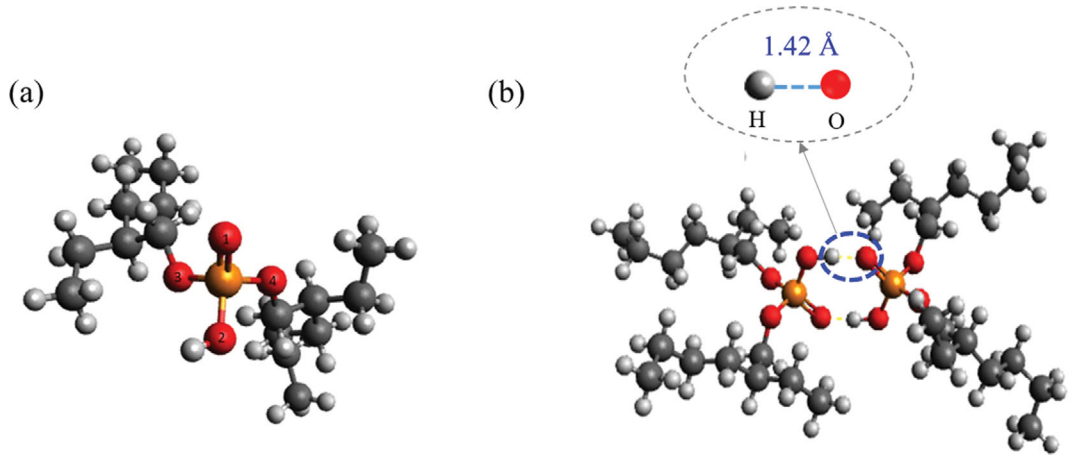

Fig. 3. The optimized molecular structure of (a) D2EHPA dissolved in kerosene and (b) dimer of D2EHPA at B3LYP/SDD level of theory.

2. Density Functional Theory Investigation

To describe more details as regards the structural chemistry, the intermolecular interaction as well as reaction energy thoroughly, DFT calculations were computed using Gaussian09program package [39]. While the molecular graphical pictures were drawn by the Avogadro program package [40,41]. In-depth discussions are as follows.

2-1. Optimized Geometry of Selected Ligand Carrier via DFT Calculation

In Fig. 3(a), the optimized molecular structure of D2EHPA dissolved in kerosene at B3LYP/SDD level of theory is presented. In Table 3, geometrical parameters are provided. Results obtained from the optimization indicate that D2EHPA formed a dimer in the kerosene diluent ($(HR)_2$) via two hydrogen bonds due to the difference in the dielectric constants. In Fig. 3(b), the interaction distance between the dimeric structures of D2EHPA of 1.42 Å is noticed. Hence, the van der Waals radii of H and O atoms are reported as 1.20 and 1.52 Å, respectively [42]. Therefore, strong intermolecular interactions exist between the dimeric structures of D2EHPA due to the interaction distance of the dimeric structures being less than the sum of van der Waals radii of H and O atoms [42]. Such results obtained proved to be in harmony with previous studies. In an inert solvent, such as kerosene, D2EHPA often completely forms a bimolecular complex (dimer molecule) via H-bonds due to an intermolecular force [43]. It has been reported that the dimeric structure of D2EHPA is formed without the dissociation of hydrogen bonding. Since there is no energy consumption for the bond-dissociation in pure state, D2EHPA is therefore favorably attracted to kerosene. Thus, as the hydrocarbon molecule gets bigger, the surface to surface contact is found to increase, allowing an increase in the intermolecular forces [37]. It is known that the bond energy is inversely proportional to the bond length. Therefore, the bond parameters as reported in Table 3 provide better insight into the molecular structural chemistry of the complex and the stability of the complex as well. Such knowledge significantly contributes to the fundamental understanding of the nature of complexes formed and the reaction mechanism occurring in the process.

Table 3. The geometrical parameters of the optimized D2EHPA at B3LYP/SDD level of theory

Bond lengths	nm	Bond angles	Å
P=O1	1.57	O1=P-O2	118
P-O2	1.69	O1=P-O3	116
P-O3	1.70	O1=P-O4	114
P-O4	1.68	P-O3-C	121
O2-H	0.98	P-O4-C	123
O3-C	1.49	P-O-H	118
O4-C	1.49		

2-2. Optimized Geometry of the Organometallic Complex Nd(III) in the Loaded Organophosphorus Ligand

The molecular geometry of the organometallic complex NdR_3·

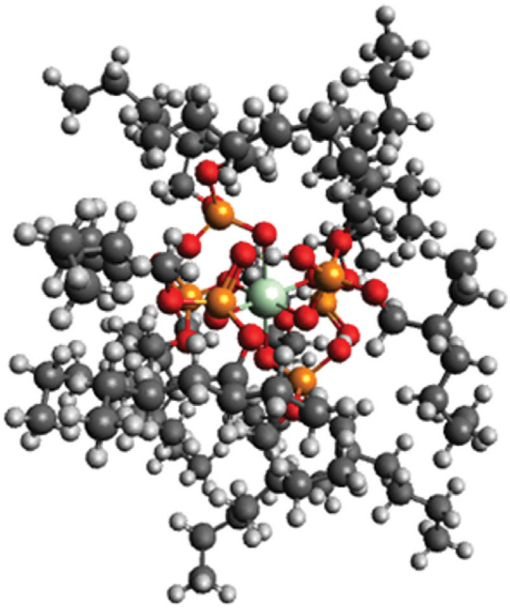

Fig. 4. Optimized molecular structure of NdR_3·$(HR)_3$ at B3LYP/SDD level of theory.

$(HR)_3$ is elucidated. Three molecules of D2EHPA dimers react with Nd(III), and $NdR_3{\cdot}(HR)_3$ is formed. A coordinated covalent bond between Nd(III) and D2EHPA carrier occurs via six oxygen atoms. In Fig. 4, the structure of the square planar bipyramid of $NdR_3{\cdot}(HR)_3$ complex is graphically shown.

3. Analysis of Reaction Mechanisms via Computational Chemistry

The investigation into reaction mechanisms is divided into two sections: extraction and stripping reactions, as described below:

3-1. Analysis of Extraction Reaction

As for the LMs phase, D2EHPA in kerosene diluent was used. During the extraction reaction, three molecules of dimeric D2EHPA ($3(HR)_2$) formed covalent bonds with Nd(III) via six oxygen atoms (Nd···O). Consequently, the square planar bipyramid of $NdR_3{\cdot}(HR)_3$ complex was produced: three protons (H^+) were lost into the aqueous phase. The calculated extraction reaction energy at B3LYP/SDD level of theory via DFT calculations was found to be 1,572.47 kJ/mol.

Next, the electrostatic surface potential (ESP) of the $NdR_3{\cdot}(HR)_3$ complex was evaluated. According to the different colors on the molecular surface, the molecular surface can be analyzed. The red surface indicated the negative charge of the oxygen atom, while the blue surface indicated the positive charge of the hydrogen atom. Herein, O atoms in the D2EHPA structure act as proton acceptor sites while oxygen and hydrogen atoms in the structure reveal the most reactive sites for both electrophilic and nucleophilic attacks, respectively. It is evident that the electrostatic attraction between O and H atoms can promote the formation of H-bond between molecules. As graphically depicted in Fig. 5, the ESP maps show that the dimer of D2EHPA occurred via two hydrogen bonds, resulting from the difference in the electrostatic charge at the center of the dimer molecule. The organometallic complex, $NdR_3{\cdot}(HR)_3$, shows the positive charge of Nd(III) in the center of the complex molecule. In general, a functional group having a negative charge and an electrostatic potential recommend the possible sites that can form a coordination bond with metal ions [44].

3-2. Analysis of Stripping Reaction

Aqueous nitric acid solution was used to strip out Nd(III) from the organometallic complex of $NdR_3{\cdot}(HR)_3$ in the loaded D2EHPA. Thus, it was found that three protons were protonated to the D2EHPA dimers, which had one intramolecular hydrogen bond. Thereby, the coordinated covalent bonds between Nd(III) and six oxygen atoms were broken. Consequently, after the protonation step, the D2EHPA dimers rearranged themselves having two intramolecular hydrogen bonds in each dimer. The calculated stripping reaction energy at B3LYP/SDD level of theory via DFT calculations was found to be −1,572.47 kJ/mol. In Fig. 6, the ESP graph of the stripping reaction is presented.

4. Separation Performance of Nd(III) Across HFSLM

4-1. Influence of Ligand Carrier Concentration

A series of experiments were carried out to examine the influ-

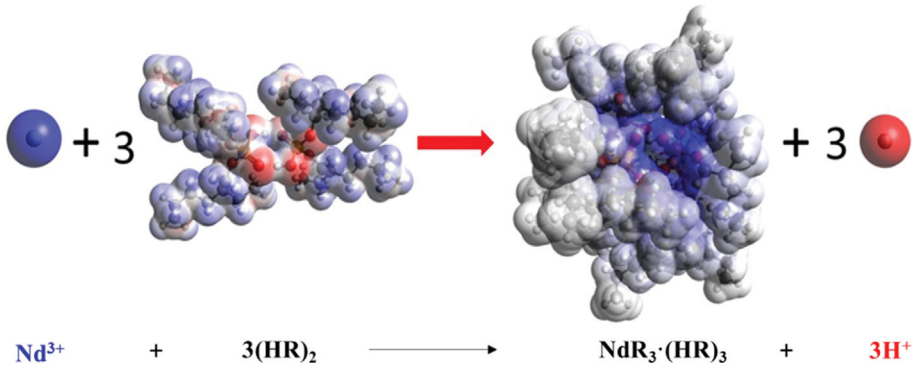

Fig. 5. Optimized reaction mechanism of Nd(III) extraction using D2EHPA as extractant at B3LYP/SDD level of theory (ESP graph).

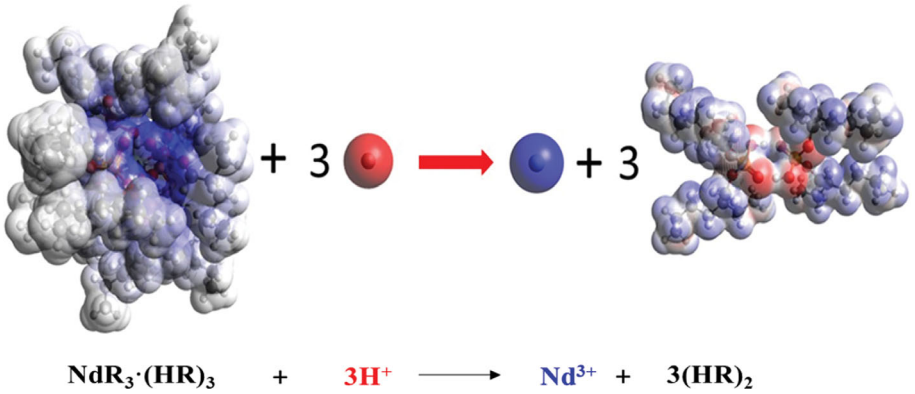

Fig. 6. Optimized reaction mechanism of Nd(III) stripping from the organometallic complex of Nd(III) in the loaded D2EHPA at B3LYP/SDD level of theory (ESP graph).

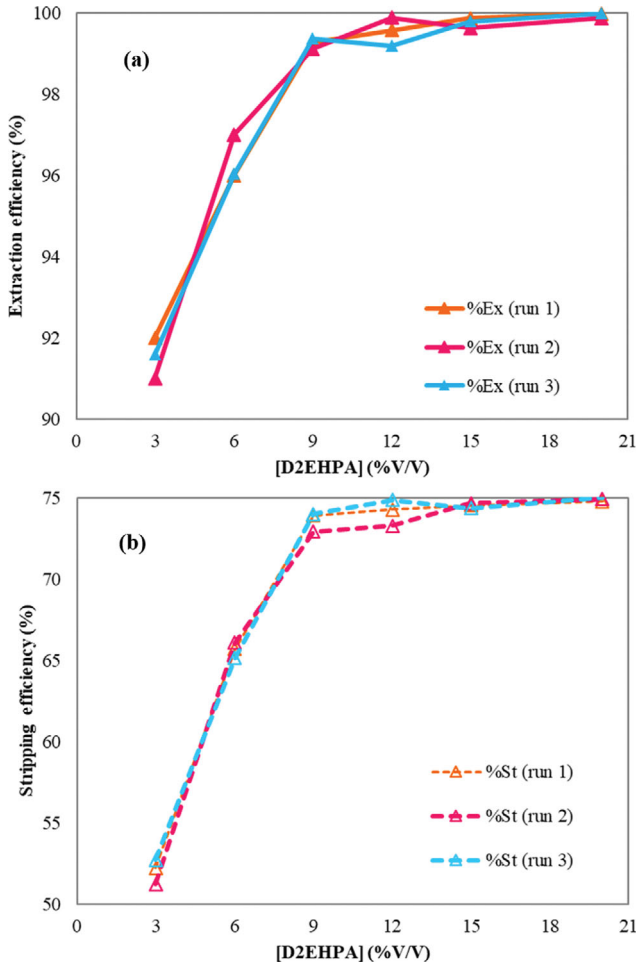

Fig. 7. Influence of carrier concentration on Nd(III) enrichment performance in terms of (a) extraction efficiency and (b) stripping efficiency (experimental conditions: aqueous feed phase; 100 mg/L of Nd^{3+}, LMs phase; D2EHPA 3-15% (V/V) dissolved in kerosene, stripping phase; 0.1 mol/L HNO_3 and Q_{feed}= Q_{strip}=200 mL/min).

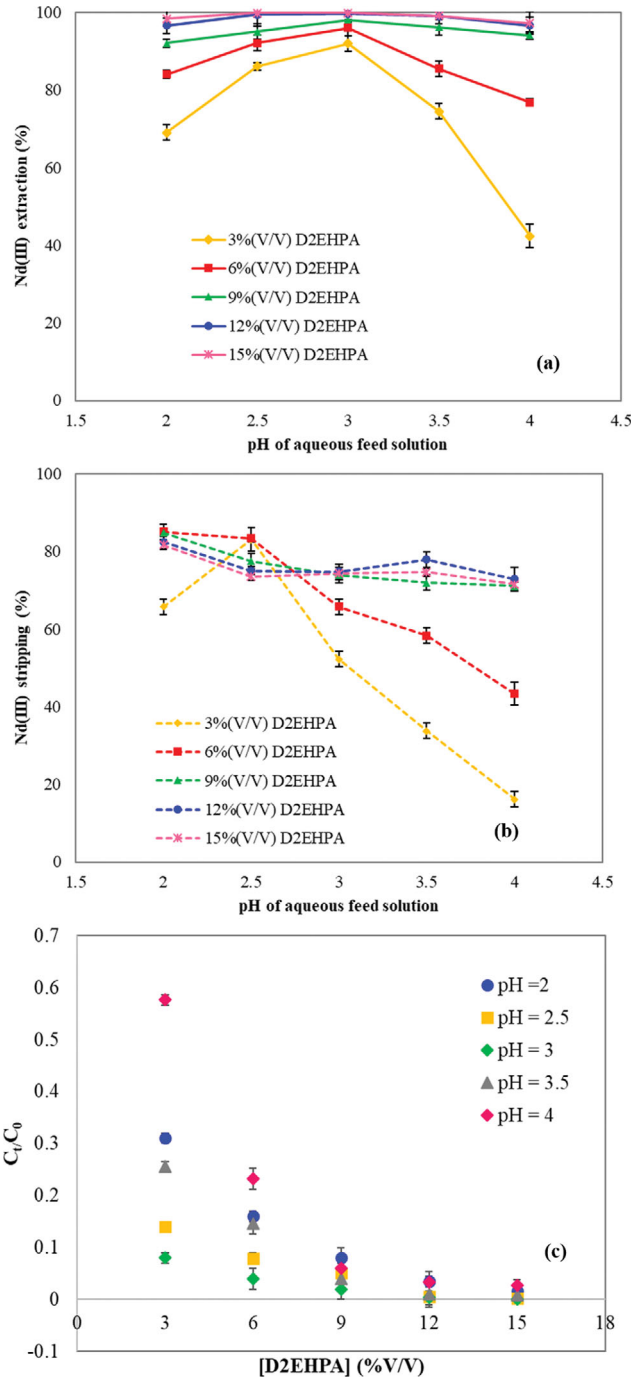

Fig. 8. Influence of aqueous feed acidity on Nd(III) enrichment performance: (a) Nd(III) extraction; (b) Nd(III) stripping and (c) Graphical plots of C_t/C_0 against carrier concentration as a function of aqueous feed acidity (experimental conditions: aqueous feed phase; 100 mg/L of Nd^{3+}, LMs phase; D2EHPA 3-15% (V/V) dissolved in kerosene, stripping phase; 0.1 mol/L HNO_3 and Q_{feed}=Q_{strip}=200 mL/min).

ence of the carrier concentration via the selected D2EHPA as extractant. The experimental data were implemented by Sulaiman N. [45]. The concentration of D2EHPA as ligand carrier was investigated in the range of 3-20% (V/V). In Fig. 7, results are given. In Fig. 7(a), when carrier concentration increased to 9% (v/v), extraction percentages of Nd(III) increased and reached maximum at 99.28%. In the case of stripping reaction (Fig. 7(b)), results proved to be similar. Such an increase in the extractability of Nd(III) can be described based on Le Chatelier's principle [46]. When ligand carrier concentration increased >9% (v/v), it had no effect on Nd(III) extraction since the extraction efficiency had almost reached maximum.

4-2. Influence of Aqueous Feed Acidity

It has been reported that in the process of REEs extraction, using organophosphorus compound as extractant is highly sensitive to the acidity of aqueous medium [47]. Thus, the influence of aqueous feed acidity was investigated in the range of pH 2-4 using HNO_3 to adjust the acidity of the aqueous feed solutions. As illustrated in Fig. 8(a) and (b), it is seen that when pH values increased from 2 to 3, the extractability of Nd(III) increased. The highest extractability yielded up to 99.87% at pH 3. The extractability of Nd(III) increased sharply at lower hydrogen ion concentration (from pH= 2-3) due to the formation of organometallic complex of Nd(III) in

the loaded D2EHPA at the f/LMs interface is favored to the equilibrium relationship (Fig. 8(c)). Such results obtained were found to be in agreement with previous work [48]. Fouad et al. [48] reported that the overall mass transfer coefficient of metal ions increased sharply with the decrease in aqueous feed acidity, suggesting the rate of formation of the organometallic complex becomes the rate-determining step. In contrast, however, at pH>3, a downward trend of Nd(III) enrichment performances was noted. This phenomenon can be described by considering the acidic carrier (D2EHPA) at the f/LMs interface [48]. Hence, the extraction of the REEs with organophosphorus compound extractant proved to be decreased with the increase in the aqueous phase acidity [47]. Therefore, pH 3 was selected as the optimum aqueous solution involving the enrichment of Nd(III). Such an outcome was in accordance with previous studies [49,50].

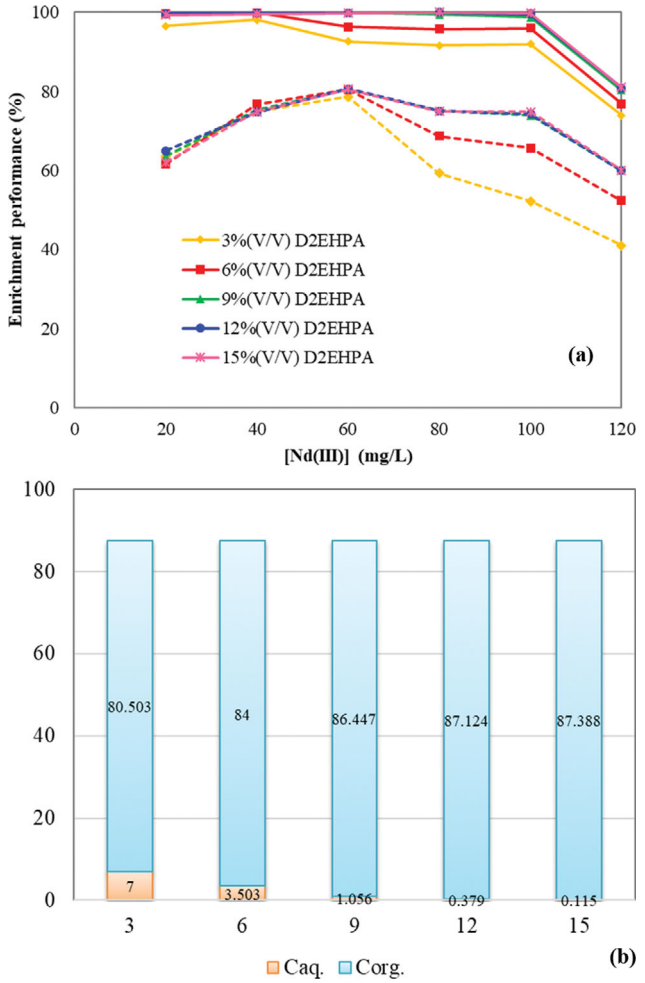

Fig. 9. Enrichment performance as a function of initial metal concentration; (a) Influence on Nd(III) extraction and recovery (experimental conditions: aqueous feed phase; 20-120 mg/L of Nd^{3+}, pH of aqueous solution; 3, LMs phase; [D2EHPA] 3-15% (V/V) dissolved in kerosene, stripping phase; 0.1 mol/L HNO_3 and Q_{feed}=Q_{strip}=200 mL/min), solid line=%extraction and dot line=%stripping and (b) the distribution of metal ions in aqueous and organic phases after extratction (at 100 mg/L of Nd^{3+}).

4-3. Influence of Initial Nd(III) in Aqueous Feed Solution

The concentration of Nd(III) in aqueous feed phase was studied in the range of 20-120 mg/L. Since, initial concentration of metals in aqueous solution prevailed the ability of the ligand carrier to be extracted into the organic phase [51]. As shown in Fig. 9(a), as concentration of Nd(III) increased, the availability of Nd(III) in the solution increased. Thus, it is seen that interfacial chemical reactions shifted in the forward direction with the result that extractability performances increased. However, at higher concentration where [Nd^{3+}]>100 mg/L, the extractability performance significantly decreased due to the limited ligand carrier availability [46,52]. Consequently, 100 mg/L of [Nd^{3+}] was chosen as the optimum condition for initial metal ions in aqueous feed solution. Thus, a downward trend of neodymium recovery (dot lines) was noticed when initial concentration of neodymium ions in aqueous feed solution was greater than 60 mg/L suggesting the limited strippant availability.

In Fig. 9(b), the graphical relationships between Nd(III) in aqueous and organic solutions is provided. The plots are conducted employing data at 100 mg/L of Nd(III). As observed, the distribution ratio proved to be increased with an increase in carrier concentration, from 3-9% (V/V). Further increase in carrier concentration (>9% (V/V)), concentration of Nd(III) in the loaded organic phase (C_{org}) was found to be slightly the same, demonstrating that it barely had no effect on the extractability of Nd(III).

4-4. Influence of Strippant Concentration

In the loaded organic phase, the process of stripping is applied to recover target metal ions. As a consequence, stripping reagents play an important role in the separation of metals from the loaded organic solution to the aqueous stripping solution. In Fig. 10, effects of concentration of HNO_3, as a stripping agent, on Nd(III) recovery are depicted. At 0.1 M HNO_3, Nd(III) can be recovered up to 73.92%. When the concentration of HNO_3 increases further, constant values of stripping percentages are observed owing to the limitation of the mass transfer area of the hollow fibers. Yoon et al. [50] reported that as the concentration of HNO_3 increased, the

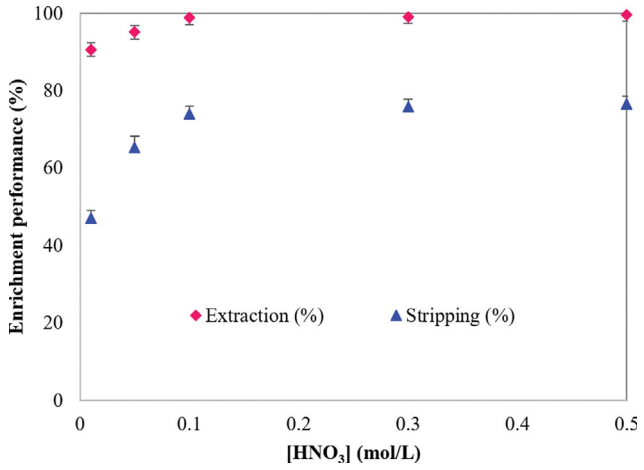

Fig. 10. Influence of strippant concentration on Nd(III) enrichment performance (experimental conditions: aqueous feed phase; 100 mg/L of Nd^{3+}, LMs phase; D2EHPA 9% (V/V) dissolved in kerosene, stripping phase; 0.01-0.5 mol/L HNO_3 and Q_{feed}=Q_{strip}=200 mL/min).

stripping efficiency of Nd(III) was found to be slightly the same. Panigrahi et al. [53] recommended that HCl and HNO_3 were highly effective reagents for the process of stripping of Nd(III) in the loaded organic phase. Liang et al. [28] ascertained that the difference in stripping percentages of Nd(III) applying HCl, H_2SO_4 and HNO_3 as stripping agents was not obvious. All three acids proved to achieve high efficiency in the process of Nd(III) recovery. Based on the stripping results obtained, 0.1 M HNO_3 was found to be the optimum condition for the stripping of Nd(III) in the loaded D2EHPA.

5. An Experimental Mechanistic Study on Extraction of Nd(III) Using D2EHPA Extractant

Generally, the extraction of metals ions using acidic organophosphorus extractants can be written as shown below [50]:

$$M_{aq}^{n+} + n(HR)_{2,\,org} \longleftrightarrow MR_n \cdot (HR)_{n,\,org} + nH_{aq}^{+} \quad (27)$$

where M=Nd, $(HR)_2$=D2EHPA and n=1, 2, 3, …, n,

As shown in Fig. 11, the stoichiometric numbers of Nd(III) and D2EHPA during the formation of the organometallic complex can be determined via the equilibrium slope analysis method [46]. By plotting log D versus log [D2EHPA], a straight line is expected. As presented in Fig. 11(a), the slope was found to be approximately equal to 3.0, indicating that 3 moles of D2EHPA are associated in the extraction of 1 mole of Nd(III). Therefore, the proposed extraction mechanism as expressed in Eq. (1) proved to be correct. Yin et al. [49] revealed that the molar ratio of Nd(III)/D2EHPA was found to be 1 : 3. Besides, in Fig. 11(b), the slopes of Log D versus Log[HNO_3] proved to be ~3 (2.7027). As seen in Eq. (5), the value of 3 was common for the stripping of Nd(III). Consequently, the value of 3 was selected since the association of 3 moles of H^+ reacts with 1 mole of Nd(III) in the loaded D2EHPA.

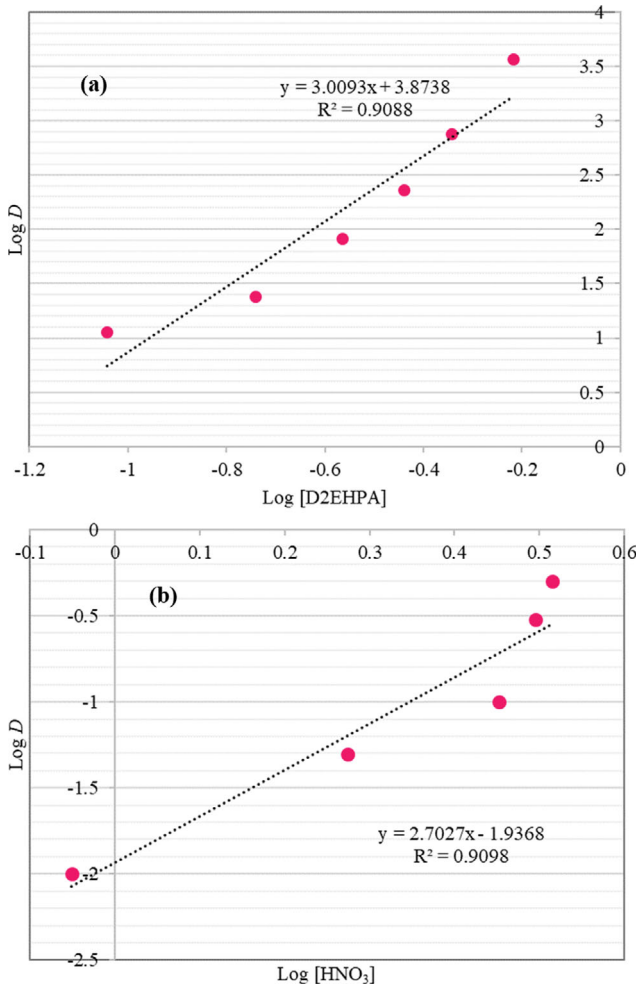

Fig. 11. Slope analysis plots: (a) logarithm plots of the distribution coefficient as a function of carrier concentration and (b) logarithm plots of the distribution coefficient as a function of strippant concentration.

The extraction mechanism of Nd(III) with D2EHPA extractant can be described as follows. First, Nd(III) is seen to coordinate with the $(HR)_2$ ligand. Hence, the complexes of NdR^{2+} that formed at the interface react with HR step by step. Next, the complexes of NdR_3 occur at the interface, releasing $3H^+$ at the same time. Finally, NdR_3 at the interface is extracted by $(HR)_2$ in the organic phase. As a result, the $NdR_3 \cdot (HR)_3$ complex is formed. It is noted that the dimer molecule exhibits the potential to coordinate with metal cations; thereby a ring chelation complex is formed. The extraction of Nd(III) via acidic organophosphorus extractant followed the cation exchange mechanism [49].

In Fig. 12, the extraction mechanism of Nd(III) using acidic organophosphorus extractant is depicted. In Fig. 12(a)-(b), the dimeric formation of D2EHPA in kerosene and the formation of Nd(III) coordinated D2EHPA complex are expressed. Based on the above description, Nd(III) is located at the center of the organometallic complex, which is formed by the chemical bond between Nd(III) and the oxygen atoms from both P=O and P···O···H. Hence, the P···O bond is acknowledged as having a short bond length and a high chemical valence, resulting in high stability of the complex structure [38]. It is significant that the reaction mechanisms simulated via computational chemistry proved to be in good agreement with the corresponding experimental data.

6. Transport Study of Active Nd(III) Using Organophosphorus Compound as Ligand Carrier

Transport properties of active Nd(III) across the HFSLM system having D2EHPA as ligand carrier can be described as follows:

6-1. Dependence of Initial Metal Concentration on Active Nd(III) Transport

(i) At the interface between feed/LMs: the net transportation rate of Nd(III) ions regarding forward reaction (extraction processes) ($J_{forward}$) is as follows: [54]

$$J_{forward} = J_{forward,\,aq.feed} - J_{backward,\,aq.feed} \quad (28)$$

Its transport rate equation is given as in Eq. (29):

$$J_{forward} = k_{forward,\,aq.feed}[Nd^{3+}]_f[(HR)_2]^3_{f/LMs} - k_{backward,\,aq.feed}[NdR_3 \cdot (HR)_3]_{LMs}[H^+]^3_f \quad (29)$$

(ii) At the interface between LMs/stripping: vice versa, the net transportation rate of Nd(III) ions regarding backward reaction (stripping processes) ($J_{backward}$) is as shown below:

$$J_{backward} = k_{backward,\,s}[NdR_3 \cdot (HR)_3]_{LMs}[H^+]^3_s - k_{forward,\,s}[Nd^{3+}]_s[(HR)_2]^3_{LMs/s} \quad (30)$$

As observed in Fig. 13, as the concentration of Nd(III) in aqueous feed solutions increased from 20 to 100 mg/L, mass fluxes of

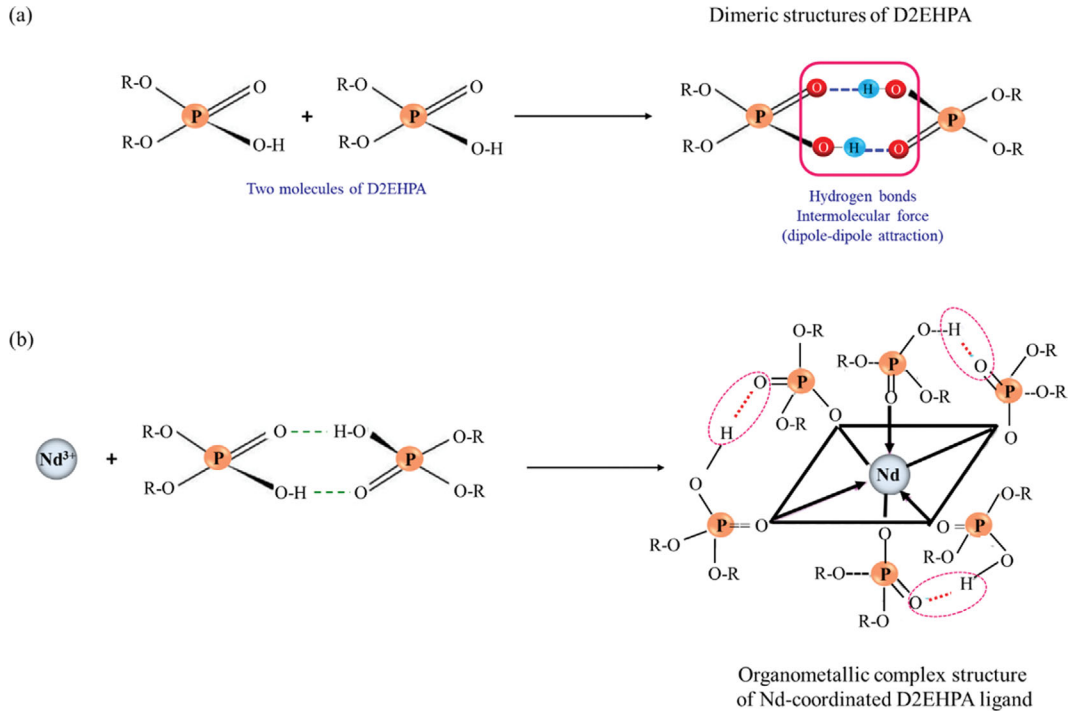

Fig. 12. Extraction mechanism of Nd(III) using acidic organophosphorus extractants: (a) the formation of dimeric D2EHPA and (b) the extracted complex of Nd in the loaded D2EHPA.

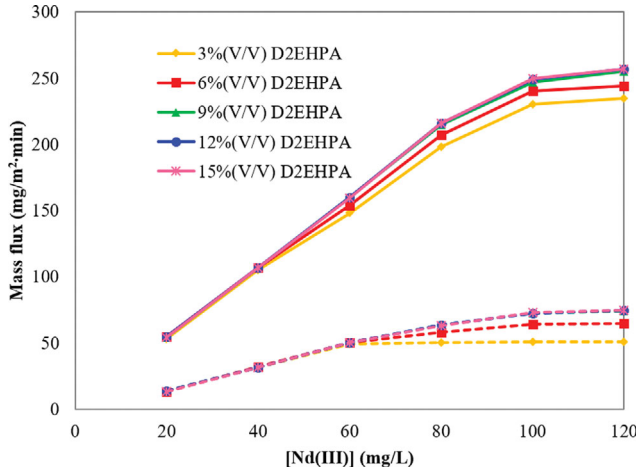

Fig. 13. Mass flux of Nd(III) as a function of metal concentration in aqueous phase (experimental conditions: aqueous feed phase; 20-120 mg/L of Nd^{3+}, pH of aqueous solution; 3, LMs phase; [D2EHPA] 3-15% (V/V) dissolved in kerosene, stripping phase; 0.1 mol/L HNO_3 and Q_{feed}=Q_{strip}=200 mL/min), solid line=extraction flux and dot line=stripping flux.

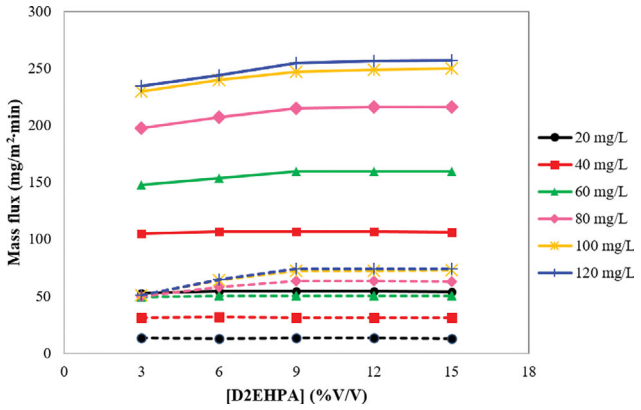

Fig. 14. Mass flux of Nd(III) as a function of ligand carrier concentration (experimental conditions: aqueous feed phase; 20-120 mg/L of Nd^{3+}, pH of aqueous solution; 3, LMs phase; [D2EHPA] 3-15% (V/V) dissolved in kerosene, stripping phase; 0.1 mol/L HNO_3 and Q_{feed}=Q_{strip}=200 mL/min), solid line=extraction flux and dot line=stripping flux.

both extraction and stripping of Nd(III) increased dramatically. Such behavior was noted over the full range of carrier concentration ([D2EHPA] 3-15% (V/V)). Meanwhile, when the concentration of Nd(III) was higher than 100 mg/L, mass fluxes of both processes were found to decrease, thereby attributing to the decrease in the distribution ratios of Nd(III). Thus, when the content of Nd(III) in the feed phase increased, it is apparent that the rate of forward reaction (extraction processes) increased.

6-2. Dependence of Carrier Concentration on the Transport Behavior of Nd(III)

In general, when carrier concentration increased, the flux of extraction reaction increased [54]. As illustrated in Fig. 14, the concentration of the ligand carrier is considered to affect the transportation flux of Nd(III) throughout the system. When a lower content of metal in the feed solution (20-40 mg/L of Nd(III)) was used, the flux of Nd(III) for both extraction and stripping reactions was slightly the same. Such an outcome was evident over the whole range of the investigated carrier concentration. In contrast, when higher

metal concentration in the aqueous feed solution (Nd(III)>60 mg/L) was implemented, the flux of Nd(III) for both reactions was found to be very different.

It is acknowledged that a ligand carrier plays a significant role regarding the transport of the target species. However, when a higher amount of carrier concentration is applied, extraction rate of Nd(III) gradually slows due to the viscosity [46,54,55].

The pertraction of target metal ions, i.e., extraction and transport through LMs, is considered to be a heterogeneous chemical reaction between ligand carrier and target metal ions. The metal fluxes, therefore, are governed by the diffusion rates of the reactants owing to the fast kinetics during interfacial reactions [55]. Accordingly, via Stokes-Einstein equation, the diffusion coefficient (D) across the LMs is expressed as shown in Eq. (31):

$$D = \frac{kT}{6\pi\eta r} \tag{31}$$

where k is the Boltzmann constant, T is the absolute temperature (K), r is the ionic radius (A^0) and η is the viscosity of the organic phase equilibrated with the aqueous phase (1×10^{-3} cP).

Hence, diffusivity is inversely proportional to viscosity. An increase in viscosity can reduce the diffusivity of the metal-carrier complex, resulting in the decrease of metal flux across the system. The term "dominant effects" has been introduced to describe such phenomena. These effects are observed due to (i) the concentration gradient of the carrier-complex species, (ii) the viscosity of the LMs and (iii) the hindered diffusion of the metal complexes caused by aggregation of the complex [30,55].

The mass flux was practically unchanged at higher concentration of carrier (as seen in Fig. 14 when D2EHPA>9% (V/V)), suggesting that the reaction kinetics strongly influenced the overall transport rate. Such results obtained were found to be in agreement with previous works [56,57]. Another reason explaining this behavior is the saturation of the interface with the molecules of complexes. Thus, at saturation concentration, the mass flux through the extraction/stripping and through the LMs is slightly the same [57].

7. Evaluation of Empirical Mass Transfer Analysis

As described in Eq. (19), mass transfer coefficients of the transported species across HFSLM can be simplified and attributed to four individual resistances. Using Eqs. (21)-(24), values of each individual coefficient can be calculated. As shown in Table 4, under optimum conditions, the individual mass transfer coefficients and their relative contribution are reported. The least value of the mass transfer coefficient indicates that mass transfer due to chemical reaction proved to be the controlling step. The relative resistances show that mass transfer in the chemical reaction is important. Thus, the resistances from the aqueous feed side, LMs and shell side were found to be much lower than that from the chemical reaction, suggesting that the mass transfer due to these three phases had little effect on the overall mass transfer process.

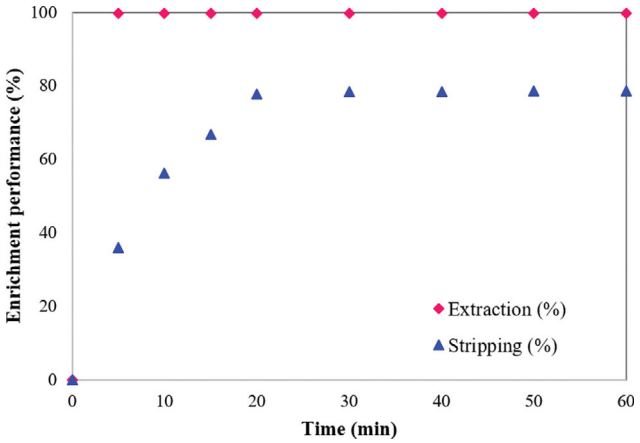

Fig. 15. Enrichment performance of Nd(III) as a function of operating time (experimental conditions: aqueous feed phase; 100 mg/L of Nd^{3+}, LMs phase; D2EHPA 9% (V/V) dissolved in kerosene, stripping phase; 0.1 mol/L HNO_3 and Q_{feed}=Q_{strip}=200 mL/min).

8. Experimental Operating Time, Operating Volume & Economic Evaluation

In Fig. 15, the operating time affecting the enrichment performance of Nd(III) is evaluated. Results show that up to 99.81% of Nd(III) was extracted within 5 min using D2EHPA 9% (V/V) as ligand carrier. When operating time increased (>5 min), the extractability of Nd(III) was found to be independent of contact time. On the other hand, stripping percentages gradually increased as operating time increased, reaching maximum stripping efficiency within 20 min. A further increase in stripping time produced the same effect; the same stripping percentages were observed. Herein, both the extraction and stripping of Nd(III) reached equilibrium at 5 and 20 min, respectively. By applying an equal flowrate for both aqueous solutions (Q_{feed}=Q_{strip}=200 mL/min), volume usage was found to be 4 L. Thus, optimum operating volume in this process is recommended as 5 L per one cycle.

In comparison with traditional solvent extraction processes, HFSLM, being low in cost, is seen to be more economical since high volumes of chemicals are needed in the solvent extraction process (A/O=1/1). While approximately 350-400 ml and 5 L of organic phase and aqueous feed solutions are used in the HFSLM process. Accordingly, the consumption of chemical reagents is significantly reduced. Based on HFSLM technology, simultaneous extraction and stripping processes can be achieved in a single-step of operation, thus reducing the cost of operation.

CONCLUSION

Under optimized conditions, D2EHPA=9% (V/V), pH of aqueous feed solution=3, initial concentration of Nd(III)=100 mg/L, stripping agent=0.1 mol/L HNO_3 and Q_{feed}=Q_{strip}=200 mL/min, enrich-

Table 4. Individual mass transfer coefficients (cm/s) and relative resistance (%) of Nd(III) through HFSLM system

k_{af}	Δ_{af}	k_{ex}	Δ_{ex}	k_{LMs}	Δ_{LMs}	k_o	Δ_o
2.10×10^{-4}	5.33	1.38×10^{-5}	81.20	1.33×10^{-4}	8.44	2.23×10^{-4}	5.02

ment performance of Nd(III) in terms of extraction and stripping percentages of Nd(III) reached 99.80% and 78.58%, respectively. Results demonstrated that HFSLM could successfully enrich Nd(III) from aqueous solutions using D2EHPA as ligand carrier. The transport of active Nd(III) due to chemical reactions across HFSLM played a major role during the process of separation. The experimental molar ratio of Nd(III)/D2EHPA was found to be 1 : 3, which proved to be in line with the optimized results obtained from computational calculations. The basis set of B3LYP/SDD level of theory showed that a coordinated covalent bond between Nd(III) and D2EHPA occurred via six oxygen atoms. It is significant that the experimental data were found to be in good agreement with the optimized structure via computational calculation. It is evident that HFSLM technology can be regarded as a green technology since the consumption of chemical reagents required in the separation processes is significantly reduced.

ACKNOWLEDGEMENTS

The authors gratefully acknowledge the financial support by Ratchadaphiseksomphot Fund (Chulalongkorn University for Postdoctoral Fellowship) and Thailand Science Research and Innovation Fund, Chulalongkorn University (CU_FRB65_ind(7)_155_21_21). Sincere thanks also go to the National e-Science Infrastructure Consortium (NECTEC) for providing computing resources that have contributed to the research results reported within this paper as well as Separation Laboratory (Department of Chemical Engineering, Faculty of Engineering, Chulalongkorn University) for their kind support.

SUPPORTING INFORMATION

Additional information as noted in the text. This information is available via the Internet at http://www.springer.com/chemistry/journal/11814.

REFERENCES

1. E. Elbashier, A. Mussa, M. Hafiz and A. H. Hawari, *Hydrometallurgy*, **204**, 105706 (2021).
2. H. Vapnik, J. Elbert and X. Su, *J. Mater. Chem. A*, **9**, 20068 (2021).
3. V. C. A. Ruiz, R. Kuchi, P. K. Parhi, J. Y. Lee and R. K. Jyothi, *Sci. Rep.*, **10**, 16911 (2020).
4. M. Gergoric, C. Ekberg, B. M. Steenari and T. Retegan, *J. Sustain. Metall.*, **3**, 601 (2017).
5. P. P. Sun, D. H. Kim and S. Y. Cho, *Miner. Eng.*, **118**, 9 (2018).
6. R. Zarrougui, R. Mdimagh and N. Raouafi, *Sep. Purif. Technol.*, **175**, 87 (2017).
7. S. N. Almeida and H. E. Toma, *Hydrometallurgy*, **161**, 22 (2016).
8. Y. Chen, H. Wang, Y. Pei and J. Wang, *Talanta*, **182**, 450 (2018).
9. S. Uchiyama, T. Sasaki, R. Ishihara, K. Fujiwara, T. Sugo, D. Umeno and K. Saito, *J. Chromatogr. A*, **1533**, 10 (2018).
10. B. Swain, S. Sarkar, K. K. Singh and A. K. Pabby, *Chem. Eng. Processing: Process Intens.*, **161**, 108300 (2021).
11. H. S. Yoon, C. J. Kim, K. W. Chung, S. D. Kim, J. Y. Lee and J. R. Kumar, *Hydrometallurgy*, **165**, 27 (2016).
12. A. C. Ni'am, Y. F. Wang, S. W. Chen, G. M. Chang and S. J. You, *Chem. Eng. Processing: Process Intens.*, **148**, 107831 (2020).
13. L. Chen, Y. Wu, H. Dong, M. Meng, C. Li, Y. Yan and J. Chen, *Sep. Purif. Technol.*, **197**, 70 (2018).
14. J. Song, T. Huang, H. Qiu, X. Niu, X. M. Li, Y. Xie and T. He, *Desalination*, **440**, 18 (2018).
15. V. Mohdee, P. Ramakul, S. Phatanasri and U. Pancharoen, *J. Environ. Chem. Eng.*, **8**, 104234 (2020).
16. M. D. Scott, J. Schorp, L. Sutherlin and J. D. Robertson, *Appl. Radiat. Isot.*, **157**, 109027 (2020).
17. D. N. Ambare, S. A. Ansari, M. Anitha, P. Kandwal, D. K. Singh, H. Singh and P. K. Mohapatra, *J. Membr. Sci.*, **446**, 106 (2013).
18. S. A. Ansari and P. K. Mohapatra, *Cleaner Eng. Technol.*, **4**, 100138 (2021).
19. T. Wannachod, P. Phuphaibul, V. Mohdee, U. Pancharoen and S. Phatanasri, *Miner. Eng.*, **77**, 1 (2015).
20. Q. Yang and N. M. Kocherginsky, *J. Membr. Sci.*, **286**, 301 (2006).
21. M. K. Hosseini, L. Liu, P. K. Hosseini, A. Bhattacharyya, K. Lee, J. Miao and B. Chen, *J. Mar. Sci. Eng.*, **10**, 1313 (2022).
22. R. Naim, G. P. Sean, Z. Nasir, N. M. Mokhtar and N. A. Safiah Muhammad, *Membranes*, **11**, 839 (2021).
23. T. Wannachod, N. Leepipatpiboon, U. Pancharoen and K. Nootong, *J. Ind. Eng. Chem.*, **20**, 4152 (2014).
24. E. G. Lewars, *Computational chemistry: Introduction to the theory and applications of molecular and quantum mechanics*, Springer, Berlin (2003).
25. L. He, L. Bai, D. D. Dionysiou, Z. Wei, R. Spinney, C. Chu, Z. Lin and R. Xiao, *Chem. Eng. J.*, **426**, 131810 (2021).
26. M. Hajji, N. Abad, M. A. Habib, S. M. H. Elmgirhi and T. Guerfel, *J. Indian Chem. Soc.*, **98**, 100208 (2021).
27. R. Cao, P. Tang, X. Yang and Z. Sun, *J. Mol. Liq.*, **357**, 119108 (2022).
28. P. Liang, W. Liming and Y. Guoqiang, *J. Rare Earths*, **30**, 63 (2012).
29. F. Kubota, M. Goto and F. Nakashio, *Solvent Extr. Ion Exch.*, **11**(3), 437 (1993).
30. K. Chakrabarty, P. Saha and A. K. Ghoshal, *J. Membr. Sci.*, **340**, 84 (2009).
31. M. Alonso, A. L. Delgado, A. M. Sastre and F. J. Alguacil, *Chem. Eng. J.*, **118**, 213 (2006).
32. P. R. Danesi, *J. Membr. Sci.*, **20**, 231 (1984).
33. Y. Tang, W. Liu, J. Wan, Y. Wang and X. Yang, *Process Biochem.*, **48**, 1980 (2013).
34. M. A. Leveque and L. L. De la, *Ann. Mines.*, **13**, 201 (1928).
35. D. Azizi and F. Larachi, *J. Mol. Liq.*, **263**, 96 (2018).
36. T. Wongsawa, N. Sunsandee, A. W. Lothongkum, U. Pancharoen and S. Phatanasri, *Fluid Phase Equilib.*, **388**, 22 (2015).
37. W. Srirachat, T. Wannachod, U. Pancharoen and S. Kheawhom, *Fluid Phase Equilib.*, **434**, 117 (2017).
38. L. E. Vargas and L. M. O. Carmona, *Minerals*, **12**, 948 (2022).
39. A. R. Allouche, *J. Com. Chem.*, **32**, 174 (2011).
40. Gaussian 09, Revision D.01, M. J. Frisch, G. W. Trucks, H. B. Schlegel, G. E. Scuseria, M. A. Robb, J. R. Cheeseman, G. Scalmani, V. Barone, B. Mennucci, G. A. Petersson, H. Nakatsuji, M. Caricato, X. Li, H. P. Hratchian, A. F. Izmaylov, J. Bloino, G. Zheng, J. L. Sonnenberg, M. Hada, M. Ehara, K. Toyota, R. Fukuda, J. Hasegawa, M. Ishida, T. Nakajima, Y. Honda, O. Kitao, H. Nakai, T. Vreven, J. A. Montgomery, Jr., J. E. Peralta, F. Ogliaro, M. Bearpark, J. J. Heyd,

E. Brothers, K. N. Kudin, V. N. Staroverov, R. Kobayashi, J. Normand, K. Raghavachari, A. Rendell, J. C. Burant, S. S. Iyengar, J. Tomasi, M. Cossi, N. Rega, J. M. Millam, M. Klene, J. E. Knox, J. B. Cross, V. Bakken, C. Adamo, J. Jaramillo, R. Gomperts, R. E. Stratmann, O. Yazyev, A. J. Austin, R. Cammi, C. Pomelli, J. W. Ochterski, R. L. Martin, K. Morokuma, V. G. Zakrzewski, G. A. Voth, P. Salvador, J. J. Dannenberg, S. Dapprich, A. D. Daniels, Farkas, J. B. Foresman, J. V. Ortiz, J. Cioslowski and D. J. Fox, Gaussian, Inc., Wallingford CT (2009).

41. M. D. Hanwell, D. E. Curtis, D. C. Lonie, T. Vandermeersch, E. Zurek and G. R. Hutchison, *J. Cheminformatics*, **4**(17) (2012).
42. D. Zhao, Y. Xiong, Y. Wang, B. Lu and H. Zhang, *Fuel*, **331**, 125704 (2023).
43. N. A. Grigorieva, I. Y. Fleitlikh, A. Y. Tikhonov, V. I. Mamatyuk, E. V. Karpova and O. A. Logutenko, *Hydrometallurgy*, **213**, 105925 (2022).
44. A. Baez-Castro, J. Baldenebro-Lopez, D. Glossman-Mitnik, H. Hopfl, A. Cruz-Enríquez, V. Miranda-Soto, M. Parra-Hake and J. J. Campos-Gaxiola, *J. Mol. Struct.*, **1099**, 126 (2015).
45. N. Sulaiman and M. Eng. Thesis, Department of Chemical Engineering, Faculty of Engineering, Chulalongkorn University, Thailand (2000).
46. V. Mohdee, C. Woraboot, K. Maneeintr, K. Nootong and U. Pancharoen, *Sep. Purif. Technol.*, **286**, 120431 (2022).
47. B. S. Dwadasi, S. G. Srinivasan and B. Rai, *Phys. Chem. Chem. Phys.*, **22**, 4177 (2020).
48. E. A. Fouad and H.-J. Bart, *J. Membr. Sci.*, **307**, 156 (2008).
49. S. H. Yin, S. W. Li, F. Xie, L. B. Zhang and J. H. Peng, *RSC Adv.*, **5**, 64550 (2015).
50. H. S. Yoon, C. J. Kim, K. W. Chung, S. D. Kim and J. R. Kumar, *J. Braz. Chem. Soc.*, 1 (2015).
51. L. Harimu, S. Matsjeh, D. Siswanta, S. J. Sentosa and I. W. Sutapa, *J. Physics: Conference Series*, **1341**, 032003 (2019).
52. B. Swain and M. Tanaka, *Chem. Eng. Commun.*, **205**, 1484 (2018).
53. M. Panigrahi, M. Grabda, D. Kozak, A. Dorai, E. Shibata, J. Kawamura and T. Nakamura, *Sep. Purif. Technol.*, **171**, 263 (2016).
54. K. R. Chitra, A. G. Galkwad, G. D. Surender and A. D. Damodaran, *Chem. Eng. J.*, **60**, 63 (1995).
55. S. Panja, R. Ruhela, S. K. Misra, J. N. Sharma, S. C. Tripathi and A. Dakshinamoorthy, *J. Membr. Sci.*, **325**, 158 (2008).
56. M. Vajda, Š. Schlosser and K. Kováčová, *Chem. Papers*, **54**(6b), 423 (2000).
57. Š. Schlosser and E. Sabolová, *Chem. Papers*, **53**(6), 403 (1999).

Supporting Information

Applicability of HFSLM for Nd(III) recovery via organophosphorus carrier: A conceptual DFT approach towards structural chemistry, mechanistic investigation and transport behavior

Vanee Mohdee*, Nisit Sulaiman*, Wikorn Punyain,†, and Ura Pancharoen*,†**

*Department of Chemical Engineering, Faculty of Engineering, Chulalongkorn University, Bangkok 10330, Thailand
**Department of Chemistry and NU-Research Center for Petroleum, Petrochemicals and Advanced Materials, Faculty of Science, Naresuan University, Phitsanulok, 65000, Thailand
(*Received 26 September 2022 • Revised 18 November 2022 • Accepted 8 December 2022*)

The drawbacks of conventional methods

Table S1. Drawbacks of conventional methodologies as applied to the recovery of REEs [1]

Separation methodology	Drawbacks
Precipitation	Sludge generated, high volumes of chemicals required
Electrocoagulation	High operational cost, short life cycle of the used anode
Flotation	Requires a post treatment
Solvent extraction	Low purity, high volumes of chemicals usage
Ion exchange	The presence of other particles which have adversely affect the efficiency, high buffering capacity
Adsorption	Produces sludge, requires a post-treatment and the presence of other ions